# Coordination of microbe-host homeostasis via a crosstalk with plant innate immunity

**Ka-Wai Ma**
Max Planck Institute for Plant Breeding Research
**Yulong Niu**
Max Planck Institute for Plant Breeding Research
**Yong Jia**
Jiangsu Key Laboratory for Microbes and Functional Genomics, Jiangsu Engineering and Technology Research Center for Industrialization of Microbial Resources, Nanjing Normal University
**Jana Ordon**
Max Planck Institute for Plant Breeding Research
**Charles Copeland**
Max Planck Institute for Plant Breeding Research
**Aurélia Emonet**
University of Lausanne
**Niko Geldner**
University of Lausanne https://orcid.org/0000-0002-2300-9644
**Rui Guan**
Max Planck Institute for Plant Breeding Research
**Sara Stolze**
Max Planck Institute for Plant Breeding Research https://orcid.org/0000-0002-1421-9703
**Hirofumi Nakagami**
Max Planck Institute for Plant Breeding Research https://orcid.org/0000-0003-2569-7062
**Ruben Garrido-Oter**
Max Planck Institute for Plant Breeding Research https://orcid.org/0000-0003-1769-892X
**Paul Schulze-Lefert** ( schlef@mpipz.mpg.de )
Max Planck Institute for Plant Breeding Research https://orcid.org/0000-0002-8978-1717

**Research Article**

**Keywords:**

**Posted Date:** September 10th, 2020

**DOI:** https://doi.org/10.21203/rs.3.rs-69445/v1

**Version of Record:** A version of this preprint was published at Nature Plants on May 24th, 2021. See the published version at https://doi.org/10.1038/s41477-021-00920-2.

# Coordination of microbe-host homeostasis via a crosstalk with plant innate immunity

Ka-Wai Ma [1] *, Yulong Niu [1] *, Yong Jia [5 #], Jana Ordon [1], Charles Copeland [1], Aurélia Emonet [2], Niko Geldner [2], Rui Guan [1], Sara Christina Stolze [4], Hirofumi Nakagami [4], Ruben Garrido-Oter [1,3] #, Paul Schulze-Lefert [1,3] #

Current affiliations

[1] Department of Plant Microbe Interactions, Max Planck Institute for Plant Breeding Research, 50829 Cologne, Germany [2] Department of Plant Molecular Biology, Biophore, UNIL-Sorge, University of Lausanne, 1015 Lausanne, Switzerland [3] Cluster of Excellence on Plant Sciences (CEPLAS), Max Planck Institute for Plant Breeding Research, Cologne, 50829, Germany [4] Protein Mass Spectrometry Group, Max Planck Institute for Plant Breeding Research, Cologne, Germany [5] Jiangsu Key Laboratory for Microbes and Functional Genomics, Jiangsu Engineering and Technology Research Center for Industrialization of Microbial Resources, College of Life Sciences, Nanjing Normal University, Nanjing 210023, China

* These authors contributed equally to this work

# Corresponding authors

Word count
Abstract 200 words
Main text 3277 words
Main Fig. 1-4
Extended Data Fig. 1-10

## Abstract

Asymptomatic plants grown in natural soil are colonized by phylogenetically structured communities of microbes known as the microbiota. Individual microbes can activate microbe-associated molecular pattern (MAMP)-triggered immunity (MTI), which limits pathogen proliferation but curtails plant growth, a phenomenon known as the growth-defense trade-off. We report that in mono-associations, 41% (62/151) of taxonomically diverse root bacterial commensals suppress *Arabidopsis thaliana* root growth inhibition (RGI) triggered by immune-stimulating MAMPs or damage-associated molecular patterns. Amplicon sequencing of bacteria *16S* rRNA genes reveal that immune activation alters the profile of synthetic communities (SynComs) comprised of RGI-non-suppressive strains, while the presence of RGI-suppressive strains attenuates this effect. Root colonization by SynComs with different complexities and RGI-suppressive activities alters the expression of 174 core host genes with functions related to root development and nutrient transport. Further, RGI-suppressive SynComs specifically downregulate a subset of immune-related genes. Pre-colonization with RGI-suppressive SynComs, or mutation of one commensal-downregulated transcription factor, *MYB15*, render plants more susceptible to opportunistic *Pseudomonas* pathogens. Our results suggest that RGI-non-suppressive and suppressive root commensals modulate host susceptibility to pathogens by either eliciting or dampening MTI responses, respectively. This interplay buffers the plant immune system against pathogen perturbation and defense-associated growth inhibition, ultimately leading to commensal-host homeostasis.

## Introduction

Ubiquitous interactions within, and between microbial communities and their plant hosts often shape host phenotypes and drive community diversification, leading to the conceptualization of plants and their associated microbes as discrete ecological units, or holobionts[1]. Analysis of *Arabidopsis thaliana* grown in different locations has shown that plants accommodate a conserved core microbiota, microbial assemblages that represent a subset of microbes from the surrounding soil seeding inocula[2-5]. While most microbiota members are commensals, a small number provide beneficial services for the host [6,7] or become pathogenic under favorable conditions. Recent studies have shed light on how specialized metabolites[8-11]and abiotic stresses[12] influence host-associated microbiota. However, how microbe-host homeostasis is maintained upon perturbation remains poorly understood.

Plants have evolved a sophisticated innate immune system to protect themselves against pathogens. One arm of this system is activated by the extracellular perception of microbe/pathogen-associated molecular patterns (M/PAMPs), e.g. the bacterial flagellin-derived epitope flg22, by cognate host pattern recognition receptors (PRRs). Both pathogenic and beneficial bacteria can carry flg22 epitope variants[13], resulting in MAMP-triggered immunity (MTI)[14,15]. MTI effectively restricts pathogen proliferation[16], but, if unrestrained, may result in plant growth penalties, a phenomenon known as the growth-defense trade-off [17]. Pathogens have evolved diverse mechanisms to suppress MTI[18], but this property is not limited to harmful bacteria, as a previous report showed commensal Alphaproteobacteria from the *Arabidopsis* root culture collection (*At*-RSPHERE)[19] can also override flg22-mediated root growth inhibition (RGI)[20]. Similarly, the beneficial rhizobacterium *Pseudomonas simiae* suppresses more than half of the MAMP-triggered transcriptional responses in mono-association with *Arabidopsis*, possibly through acidification of the rhizosphere[13,21]. However, how plants tolerate a rich diversity of commensals without compromising effective resistance to pathogens is unknown. Here, we used a bottom-up approach to show that phylogenetically diverse root commensals can modulate plant immunity and their combined interactions in community contexts coordinate commensal-host homeostasis under pathogen challenge[22,23] .

## Results

### Taxonomically widespread ability of root commensals to interfere with defense-associated growth inhibition

To facilitate screening of individual root commensals of the *At*-RSPHERE culture collection, we took advantage of a flg22-hypersensitive line, *pWER::FLS2-GFP*[24,25], in which the flg22 receptor *FLS2* is overexpressed but restricted to the root epidermis. This hypersensitivity leads to an enhanced signal-to-noise ratio for flg22-mediated RGI (Extended Data Fig. 1a). After three weeks of co-culturing with individual bacterial isolates and flg22, 41% of the strains (62 out of 151) were found to interfere with RGI. RGI-suppressive activity was detected across all four phyla of the microbiota – Actinobacteria, Proteobacteria, Bacteroidetes, and Firmicutes – but was overrepresented among Actinobacteria and Gammaproteobacteria commensals (Fig. 1a). Viable plate counting confirmed that the RGI non-suppressive strains still colonize roots in mono-associations (Extended Data Fig. 1b). In contrast, only three strains, *Streptomyces* strains 107 and 187, and *Pseudomonas* 401, had detrimental impacts on *Arabidopsis* in mono-associations, with *Pseudomonas* 401 most severely compromising plant growth (Extended Data Fig. 1c).

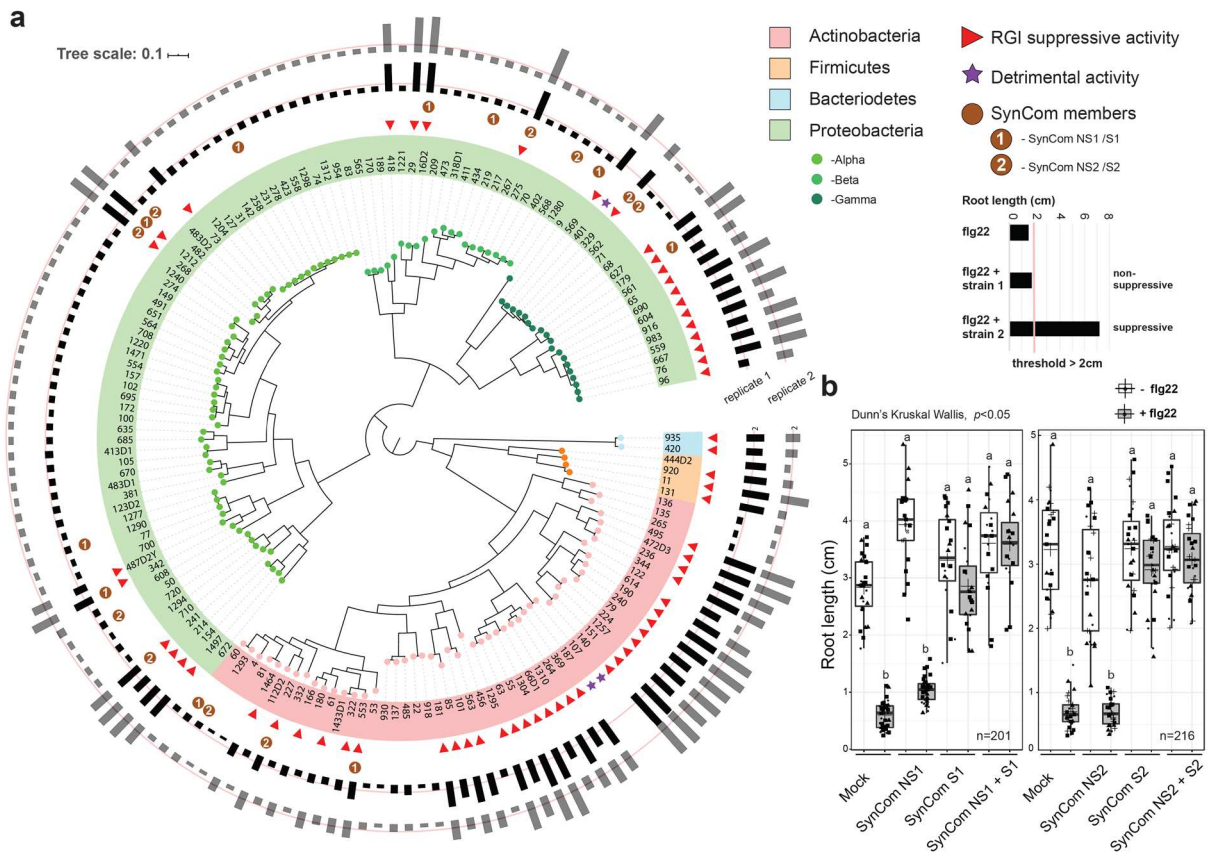


**Figure 1**

*At*-RSPHERE root commensals exhibit strain-specific variation to suppress flg22-mediated RGI in *pWER::FLS2-GFP* plants. (a) Phylogenetic tree showing the distribution of strains exhibiting RGI suppressive activity. The outer rings represent root lengths of 3-week old plants treated with 1µM flg22 and individual strains ($OD_{600}$=0.0005). The threshold for suppressive activity is indicated by the red line i.e. root length > 2cm. (b) The impact of 4 independent 5-member SynComs (Table S1) differential in RGI suppressive activity on flg22-mediated RGI. Shapes correspond to biological replicates. Different letters indicate statistical significance.

To examine whether root-derived bacteria were also able to suppress RGI elicited by an endogenous plant-derived danger-associated molecular pattern (DAMP), we treated plants with the DAMP *At*pep1, which induces RGI and immune responses[26]. Using *At*pep1-treated Col-0 wild type (WT) plants, we found that 12 out of 13 suppressive strains, representing members from diverse taxa, retained the capacity to interfere with RGI, while none of the eight non-suppressive strains elicited this effect (Extended Data Fig. 2a). Thus, phylogenetically diverse root commensals can suppress both DAMP- and MAMP-induced RGI. One isolate, *Caulobacter* strain 342, suppressed flg22- but not *At*pep1-mediated RGI (Extended Data Fig. 2b), suggesting the existence of at least two modes of RGI suppression, one interfering with both MAMP- and DAMP-induced RGI, the other possibly specific to flg22 perception.

Although germ-free *pWER::FLS2-GFP*[24] plants respond to flg22 treatment with enhanced RGI compared to Col-0 on synthetic medium, no growth differences were noted between these two genotypes when grown in natural soil (Extended Data Fig. 2c). Given that root growth in natural soil likely proceeds in the face of chronic exposure to MAMPs and DAMPs as well as colonization by both suppressive and non-suppressive commensals, we speculated that the aforementioned RGI suppression phenotype might act as a dominant community trait. To test this hypothesis, we composed four independent but taxonomically similar 5-member synthetic communities (SynComs)

with contrasting capacities for RGI suppression, i.e., non-suppressive SynComs (SynCom NS1 and NS2) and suppressive SynComs (SynCom S1 and S2; Table S1). We observed RGI-suppressive activity in plants inoculated with the suppressive SynComs but not with the non-suppressive SynComs. Furthermore, full RGI suppressive activity was retained when these commensals were combined as 10-member SynComs (Fig. 1b). A recent study showed that auxin-mediated RGI could be rescued by *Variovorax* commensals[27]. However, our four tested SynComs neither induced RGI to a level comparable to flg22 treatment, nor did the presence of *Variovorax* 434 in SynCom NS1 rescue the flg22-mediated RGI phenotype (Fig. 1b). Therefore, we conclude that RGI is mainly caused by flg22 treatment and is widely suppressed by *At*-RSPHERE members that function dominantly in our setup.

We speculated that the co-occurrence of RGI-non-suppressive and suppressive strains might reflect a need for commensal microbes to dampen plant immunity to balance root growth and defense trade-offs. Thus, we asked if a single suppressive strain is sufficient to achieve full RGI suppression. We found that the addition of diverse individual suppressive strains to a 5-member non-suppressive SynCom resulted in only partial RGI suppression (Extended Data Fig. 2d). This result suggests that the identity of suppressive commensals, and the input proportion of suppressive to non-suppressive strains affect RGI suppression capacity quantitatively.

Previously, commensal *Pseudomonas spp.* in mono-associations were shown to acidify the growth medium rendering plants insensitive to flg22[21]. To determine if acidification is responsible for RGI suppression by our SynCom, we measured the pH of growth medium of plants co-inoculated with different SynComs and observed average reductions in pH from 5.18 in mock treatment to 4.62 and 3.97 in the presence of a SynCom S1 and NS1, respectively. This lack of correlation between RGI suppression and growth medium acidification suggests that this mechanism is unlikely to explain suppression in our community setup. Intriguingly, *hrcC*, a gene required to form a functional type three secretion system in pathogenic *Pseudomonas*, is dispensable for RGI suppression mediated by suppressive *Pseudomonas* strain 569 (Extended Data Fig. 2e-f). Further, the culture filtrate of an Actinobacteria member, *Janibacter* 101, suppressed both flg22 and *At*pep1-induced RGI (Extended Data Fig. 3a-c). Heat treatment and filtration of the culture filtrate showed that the molecule(s) responsible is heat-labile and is retained by a 3kDa filter (Extended Data Fig. 3d). Mass spectrometry analysis revealed that the filtrates of two out of five tested suppressive commensals elicited a significant reduction of intact flg22 peptide (Extended Data Fig. 3e). Thus, the ability of some strains to suppress MTI resembles the activity of pathogenic bacteria[28] and is associated with an ability to modify/degrade flg22 peptide. Together, these data suggest diverse mechanisms in commensals to suppress elicitor-mediated RGI.

## Activation of immunity shapes root microbiota establishment

To determine if plant immunity affects microbiota establishment, we performed reconstitution experiments with gnotobiotic plants grown in an agar matrix. We designed three taxonomically similar SynComs with contrasting RGI suppression capacities for community profiling experiments with strain-specific resolution (total of six SynComs; Table S1). Principal Coordinate Analyses (PCoA) of Bray-Curtis dissimilarities revealed that root-associated bacterial communities were distinct from the corresponding unplanted or planted matrix samples (Extended Data Fig. 4), regardless of the SynCom composition and plant genotypes (Col-0 and *pWER::FLS2-GFP*). Constrained PCoA revealed that flg22 treatment elicited a consistent community shift in plants inoculated with non-suppressive SynComs, while samples from those inoculated with suppressive SynComs remained together. Consistent with a dominant effect of RGI suppression, roots inoculated with 10-member mixed communities (suppressive plus non-suppressive SynComs) were not affected by flg22 treatment (Fig. 2a-c, Extended Data Fig. 5a-c).

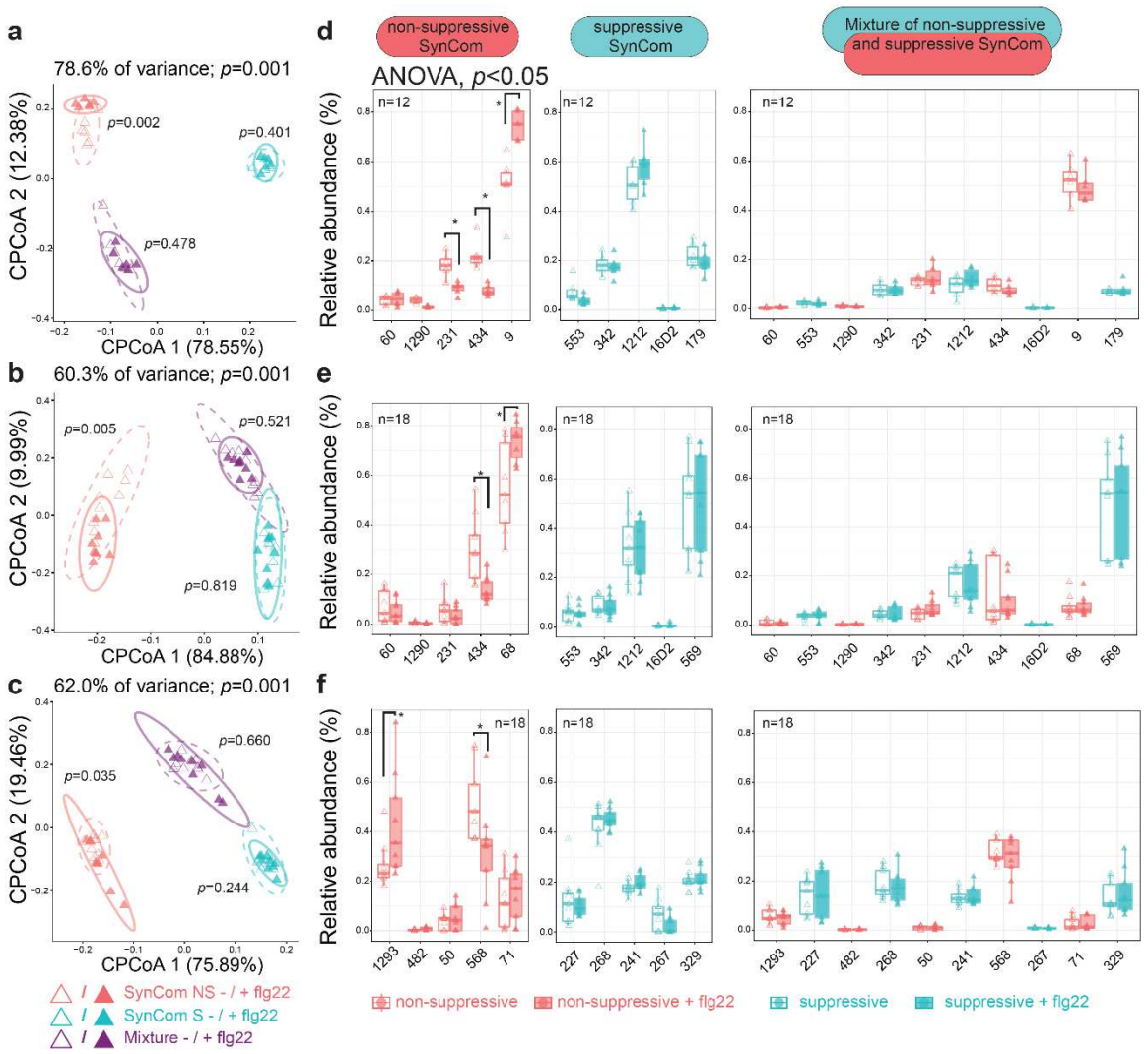


**Figure 2**

Activation of immunity by flg22 affects community establishment. (a-c) Constrained coordination of the microbial profile of *pWER::FLS2-GFP* root samples showing the corresponding community shift of non-suppressive SynCom upon flg22 treatment. Ellipses correspond to Gaussian distributions fitted to each cluster (95% confidence interval). *p*-values next to ellipses indicate statistical significance based on a PERMANOVA test between untreated and flg22-treated samples of each SynCom (permutation=999). (d-f) Relative abundance of strains upon flg22 treatment. Experiment 1: (a,d); experiment 2: (b,e); experiment 3: (c,f). Values in bracket are eigenvalues explained by the Principal Component (PC). Asterisks indicate statistical significance.

To dissect the contribution of individual strains to the overall community shift, we quantified the relative abundance (RA) of individual strains. The detection of non-suppressive commensals as the most abundant strains in the mixed SynComs suggests that the ability to dominate in a community is not necessarily coupled to RGI suppression (Fig. 2d-f, Extended Data Fig. 5d-f). However, the RA of specific strains in a community was impacted by plant immunity. For example, flg22 treatment led to altered RA of *Pseudomonas* 9/68 (up) and *Variovorax* 434 (down), while *Microbacteriaceae* 60 was unaltered (experiment 1, 2). Similarly, flg22 treatment altered the RA of *Microbacteriaceae* 1293 (up) and *Comamonadaceae* 568 (down), while *Pseudomonas* 71 was unaffected (experiment 3; Fig. 2d-f). A similar trend was also detected in Col-0 (Extended Data Fig. 5d-f), though the effect was more pronounced in *pWER::FLS2-GFP* plants, possibly due to enhanced MTI and/or altered root architecture. In addition, we found that flg22 treatment reduced within-sample diversity of non-

suppressive SynComs, (experiment 1, 2; Extended Data Fig. 5g), suggesting that immune activation can affect the distribution of specific strains in community contexts.

## Root transcriptomic changes and dampening of immunity by suppressive SynComs

Although flg22-mediated RGI is closely associated with immune activation, its role as a *bona fide* immune output is unclear. Next, we sought to explore how inoculation with suppressive or non-suppressive SynComs affected the root transcriptome of plants treated with flg22 grown on an agar matrix (Table S2 and S3). Principal component analyses (PCA) at the transcriptome level revealed distinct expression patterns between Col-0 plants inoculated with live bacteria compared to germ-free plants (PC1, 20% variance; Fig. 3a). Interestingly, the transcriptional output of roots inoculated with these two taxonomically similar SynComs were clearly differentiable after two weeks of co-cultivation, even in the absence of flg22 treatment (triangles, Fig. 3a). In addition, we observed a separation according to the immune status of the plants, triggered by flg22 exposure, in all samples treated with heat-killed bacteria as well as with the non-suppressive SynCom (PC2, 7% variance; Fig 3a). By contrast, MAMP treatment of plants colonized by the suppressive SynCom did not elicit significant changes. Independent transcriptome experiments using *pWER::FLS2-GFP* plants confirmed these results (Extended Data Fig. 6 and Table S2).

Next, we performed *k*-means clustering of differentially expressed genes (DEGs) involved in flg22 response, SynCom response, or both (Fig. 3b and Table S3). We observed three large clusters (2,221 DEGs) that were induced (c4 and c5) or suppressed (c8) by live bacteria independent of flg22 treatment (Fig. 3b-c). Gene ontology (GO) enrichment analyses showed that the SynCom-responsive clusters were primarily enriched in functions related to detoxification, root development, nutrient transport, and response to hypoxia (Extended Data Fig. 7). To determine whether similar GO terms could also be identified in experiments with more complex SynComs, we compared our data with two independent *Arabidopsis* root transcriptome studies that employed SynComs consisting of both suppressive and non-suppressive commensals (35 members, Teixeira et al., co-submitted manuscript; 115 members[29]). Despite differences in technical setups and SynCom complexities, we identified 174 common SynCom-responsive DEGs in the absence of flg22 that were related to the same biological functions mentioned above (Extended Data Fig. 8 and Table S4).

Importantly, we found a flg22-inducible cluster (c3), which was significantly upregulated by the non-suppressive SynCom but downregulated by the suppressive community (Fig. 3b-c), in a pattern matching the RGI phenotype of the plant (Fig. 1b) and the bacterial community shifts (Fig. 2). As expected, a portion of defense-related genes were enriched in c3, e.g. *PER5*, *FRK1* and *RBOHD* (70 genes; Fig. 3b). However, additional defense-related DEGs were found outside c3 and were upregulated by flg22 treatment even in the presence of the suppressive SynCom (348 genes; Fig. 3b). Previously characterized examples include regulators of antimicrobial camalexin, e.g., *MYB51*[30,31] (c5); systemic acquired resistance, e.g. *FMO1* (c5) and *SARD1* (c1)[32,33]; and endogenous peptides amplifying MTI e.g. *PIP1* and *PIP2*[34] (c5; Fig. 3b). Recent work showed that MAMP responsiveness in germ-free roots was gated by the expression of damage-induced PRRs[35]. However, the sustained expression of *FLS2* (c1) in the presence of SynComs indicates that RGI suppression is not due to *FLS2* downregulation (Fig. 3b). An independent study by Teixeira *et al*. also identified a cluster of DEGs that was highly induced in axenic *Arabidopsis* by flg22-treatment but suppressed by the presence of a 35-member SynCom consisting of suppressive and non-suppressive root commensals (Extended Data Fig. 9). Remarkably, this cluster showed the largest overlap with our cluster c3 with 58 common DEGs (at least 21 were defense-related) that were downregulated by both SynComs (Extended Data Fig. 9).

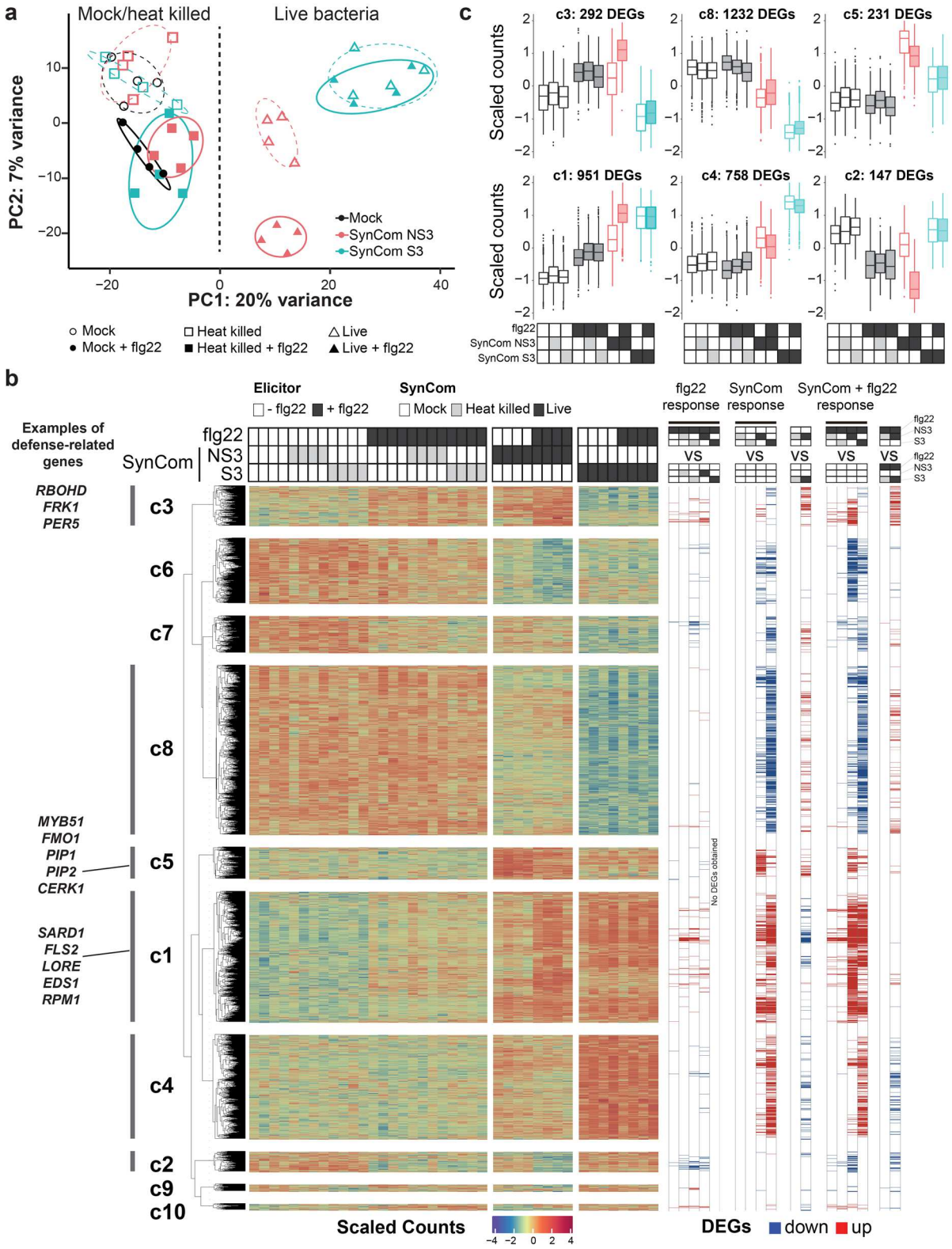


**Figure 3**

SynCom colonization and flg22 treatment induce root transcriptomic changes in WT Col-0 plants. (a) PCA plot separating samples inoculated with SynComs and flg22. Ellipses correspond to *t*-distributions fitted to each cluster (70% confidence interval). (b) Heat map (middle) and DEGs (Table S3) obtained by pairwise comparison (right). *k*-means clusters (*k* = 10) are marked on the left. (c) Scaled counts of transcripts in six clusters and their expression patterns upon treatments. The corresponding transcriptome data of *pWER::FLS2-GFP* plants are presented in Fig. S6 and table S2.

We further validated our findings by examining the expression of two flg22-inducible defense marker genes[12,24,36] in roots of *Arabidopsis* by qPCR in the presence of other suppressive SynComs. *PER5* and *FRK1* remained significantly elevated two weeks after co-inoculation with flg22 and a non-suppressive SynCom but not with a suppressive SynCom (Extended Data Fig. 10a). A non-suppressive SynCom alone also significantly induced their expressions, indicating that non-suppressive commensals stimulate specific root immune responses. As expected, a 10-member mixed SynCom did not significantly induce the expression of the two tested marker genes (Extended Data Fig. 10b). To determine if MTI has a direct impact on commensal proliferation independent of any microbe-microbe interactions, we focused on transcription factors (TFs) and investigated the contributions of the top three candidates identified in our dataset, *WRKY30*, *MYB15*, and *WRKY28* (cluster c3; Extended Data Fig. 10c-d). Null mutants of *WRKY30* and *WRKY28* have not been reported, and our attempts to knock-out these TFs *via* CRISPR failed, suggesting that these genes are essential for plant viability[37,38]. We therefore focused on *MYB15*, a positive regulator of defense against the foliar pathogen *Pto*DC3000[39]. In *myb15-1* plants, elimination of this single TF led to a significantly enhanced proliferation of the detrimental strain *Pseudomonas* 401 and the commensal *Variovorax* 434 ($p<0.05$, Extended Data Fig. 10e-f), which also showed a reduced RA upon flg22 treatment in community contexts (Fig. 2d-e). Together, amplicon sequencing and transcriptome data support the idea that colonization of specific root commensals is affected by host MTI, which can be attenuated by suppressive strains.

## Suppressive and non-suppressive commensals differentially impact plant susceptibility to opportunistic pathogens

Since a subset of commensals dampens root immune responses, we hypothesized that colonization with a suppressive SynCom might render plants more susceptible to opportunistic pathogens. We identified three detrimental strains from *At*-RSPHERE. In particular, *Arabidopsis* plants inoculated with *Pseudomonas* 401 exhibited reduced growth and accumulated pigments in shoots reminiscent of stress-inducible anthocyanins (Extended Data Fig. 1c), which indicates its pathogenic potential in a laboratory environment. Consistent with the fact that 401 was originally isolated from healthy and asymptomatic *Arabidopsis* roots colonized by a diverse microbial community, the detrimental effect was attenuated when plants were colonized by our SynComs. Interestingly, the attenuation is stronger when plants were co-colonized with the non-suppressive SynCom compared to the suppressive SynCom (Fig. 4a). Recent reports suggest a positive correlation between disease progression in natural *Arabidopsis* populations and bacterial biomass[40,41]. To determine whether *Pseudomonas* 401 virulence is related to enhanced plant colonization, we quantified its absolute abundance on *pWER::FLS2-GFP* pre-colonized with suppressive or non-suppressive SynComs. Plants already colonized by suppressive SynComs harbored significantly higher 401 titers compared to plants pre-colonized with non-suppressive SynComs (Fig. 4b-c). Interestingly, this SynCom-dependent difference appeared to be limited to roots since 401 growth in shoots was similarly restricted by co-colonization with either community (Fig. 4b-c). Furthermore, individual SynCom strains did not antagonize 401 *in vitro* (Extended Data Fig. 10g), suggesting that the underlying growth differences are unlikely to be the result of antibiosis.

To determine whether SynComs modulate plant susceptibility to a characterized opportunistic pathogen prevalent in natural *A. thaliana* populations, we inoculated plants with the opportunistic *Pseudomonas* leaf pathogen OTU5 (isolate p5.e6) (Fig. S1c). Plants colonized by suppressive SynComs supported higher growth of *Pseudomonas* OTU5 compared to plants colonized by non-suppressive SynComs, and this SynCom-specific effect was again observed only in roots but not in shoots (Fig. 4b-c). Together with the RNA-Seq data, these results suggest that pre-colonization with non-suppressive

SynComs activated root immunity and this correlates with reduced growth of the tested opportunistic pathogens, whereas suppressive SynComs failed to provide pathogen protection.

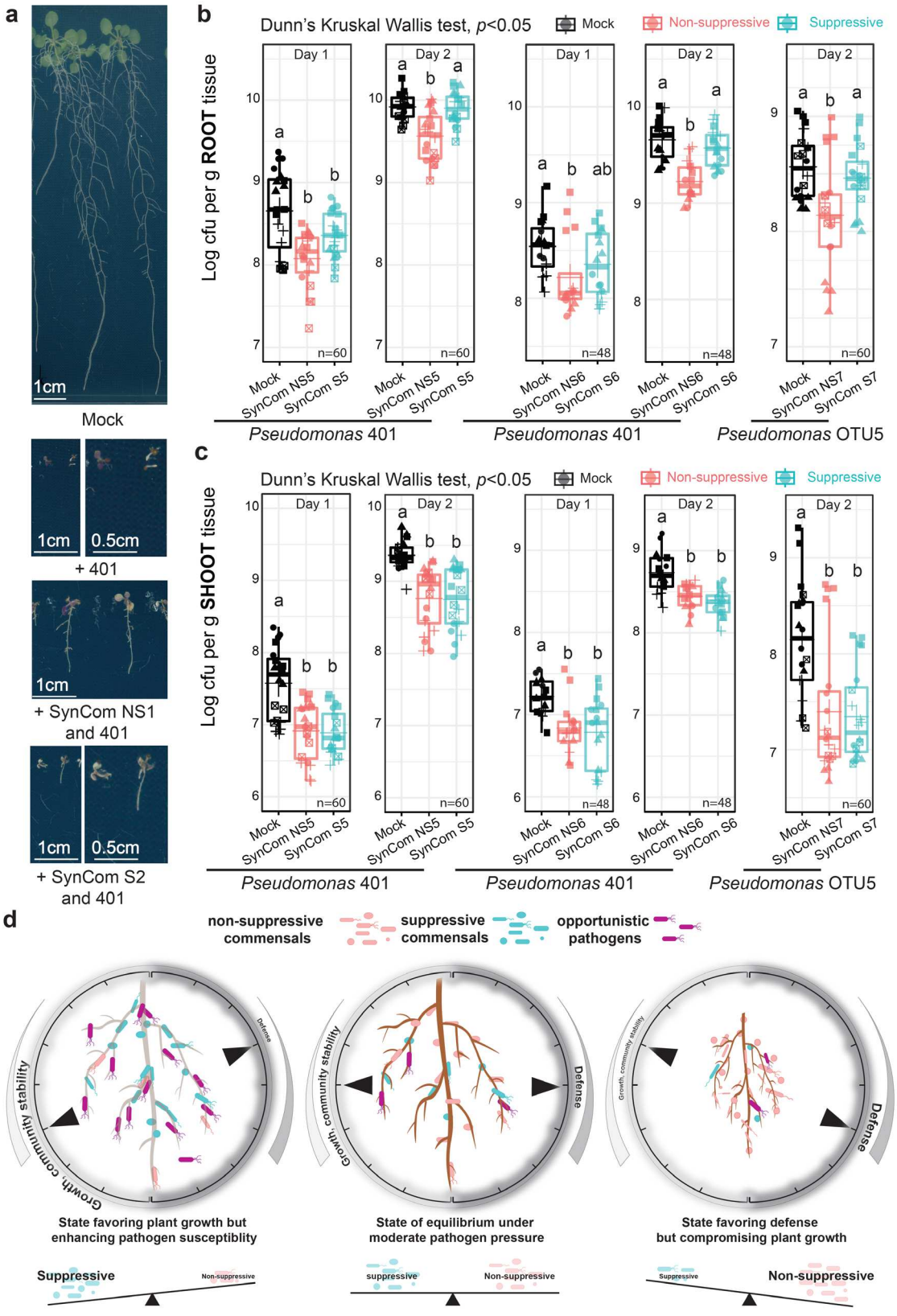


**Figure 4**

Imbalance of specific bacteria impacts plant susceptibility to opportunistic *Pseudomonas* pathogens. (a) Symptoms of 3-week-old WT plants germinated with the indicated SynCom and *Pseudomonas* 401. Bacterial titer of *Pseudomonas* 401 and OTU5 on the roots (b) and shoots (c) of *pWER::FLS2-GFP* plants pre-colonized

with the indicated SynComs for 2 weeks. Shapes correspond to biological replicates. Different letters indicate statistical significance. (d) The "rheostat model" proposes that the balance between non-suppressive and suppressive strains integrates with plant innate immunity and buffers the system against pathogen challenge and defense-associated trade-off.

## Discussion

In nature, a subset of soil-dwelling bacteria colonizes roots seemingly without influencing host traits, and are thus often considered as commensals. Using a bottom-up approach, we show here that phylogenetically diverse commensals, representing the core of the *Arabidopsis* root microbiota[19], share the capacity to suppress host defense responses, a microbial trait that is dominant in our community setup, and is thus easily overlooked in nature. To date, information on *Arabidopsis* root transcriptomic changes evoked by commensals are limited to mono-associations[13,20], leaving a gap in our understanding of how plant roots respond to commensal communities that can reach a steady-state as early as 13 days after inoculation[42]. We unexpectedly found that after 2 weeks, root colonization by taxonomically similar commensal SynComs, differing in their capacity to suppress RGI, elicited 2,221 DEGs (cluster c4, c5, c8) with remarkable overall similarity. These changes associated with presumably steady-state SynComs contrast with the subtle response to heat-killed SynComs or flg22 treatment alone, reflecting an impact of active commensal colonization on host transcriptional outputs beyond plant responses to chronic exposure to MAMPs. Further, we observed robust enrichment of specific GO terms related to root development, nutrient transport, response to hypoxia and detoxification across experimental setups and SynCom complexities([29], Teixeira *et al.*, 2020). Indeed, rhizobacteria alone are known to modulate root traits[20,43,44]. In return, root-secreted photoassimilates feed up to 20% of root-associated bacteria [45], which served as sources of organic carbon that limit bacterial growth[46]. We thus speculate that enrichment of these GOs is associated with altered nutrient flux, and reduced oxygen due to microbial respiration in roots. Although our SynComs are taxonomically diverse with predicted varied metabolic repertoires[19,47], convergence to core transcriptomic outputs indicate integrated responses to a state of "community commensalism".

The zigzag model of the plant immune system proposes that effective resistance is the result of quantitative outputs above a certain threshold following MAMP perception[18]. Colonization by suppressive SynComs led to the down-regulation of a subset of flg22-induced genes (Fig. 3, cluster c3), whereas colonization by non-suppressive SynComs alone stimulated them and further upregulated their expression together with flg22. Thus, the responsiveness of these defense-associated genes to SynCom colonization differs greatly with respect to the ability of the bacterial community to suppress RGI. However, roots in nature are co-colonized by both groups of commensals and our experiments point to a quantitative output that is dependent on their ratio. Intriguingly, recent studies reported that 42%[21] and 28% (Teixeira et al., 2020) of commensals from two other *Arabidopsis* root-derived culture collections quench early and late flg22-induced responses in mono-associations, respectively[21]. Together with our study, this confirms a potential of the root microbiota to modulate plant growth-defense traits.

We hypothesize that the imbalance between non-suppressive and suppressive commensals might reduce plant fitness under stress conditions. Indeed, plants pre-colonized by suppressive SynComs are as susceptible as germ-free plants to opportunistic *Pseudomonas* pathogens, whereas plants associated with non-suppressive SynComs are more resistant but prone to MAMP-induced RGI. The observed defense-associated community shifts and potentially reduced alpha-diversity might hinder provision of microbiota-derived beneficial services [48], or exert detrimental impact on the host under dysbiosis[49]. We thus propose a rheostat model (Fig. 4e) in which a balance between commensals with contrasting MTI modulating activities constitutes an integral feature of the holobiont to buffer

plant resistance to pathogen perturbation and defense-associated growth reduction. Consequently, this allows community coexistence, and eventually establishes microbe-host homeostasis. Accordingly, their ratio will impact the amplitude and/or might set the threshold for effective resistance in the zigzag model. Plants in nature are influenced by fluctuating stresses and are colonized by more diverse microbial communities that modulate plant physiology through multiple mechanisms, including the modulation of phytohormone signaling[27,50]. It will be a future task to test whether the rheostat model also applies to communities with different traits to alleviate abiotic stresses.

**Acknowledgement**

The authors would like to thank Anna Lisa Roth and Christina Philipp for technical support, Dr. Bruno Huettel from the Genome Centre of MPIPZ for the preparation and sequencing of RNA-Seq libraries, Anne Harzen from the core proteome facilities for the preparation of mass spectrometry samples. We thank Dr. Nicole Clay and Dr. Detlef Weigel for providing *Arabidopsis myb15-1* seeds and strain OTU5, respectively. We thank Dr. Jeff Dangl and Dr. Paulo Teixeira for sharing their unpublished data. This research was funded by the Deutsche Forschungsgemeinschaft (DFG, German Research Foundation) under Germany´s Excellence Strategy – EXC-Nummer 2048/1– project 390686111 and SPP 2125 DECRyPT to R.G.O. and P. S.-L.. K.W.M. was supported by postdoctoral fellowships from EMBO (ALTF 1144-2017) and the Alexander von Humboldt Foundation. We also thank Neysan Donnelly for reading and editing of the manuscript.

**Authors contribution**

K.W.-M., and P.S.-L. conceptualized the initial project. K.W.-M., R.G.-O. and P.S.-L. designed the experiments. K.W.-M. performed the initial screening of RGI suppressive members; 16S amplicon sequencing with the help of C.C., J.O., and Y.J.,; RNA-Seq experiments; and inoculation experiments involving strains 401, 434 and OTU5 with the help of J.O. and Y.J.. Y.N. performed RNA-Seq data analyses and developed all related pipelines for GO term enrichment, network studies and cross-studies comparisons. K.W.-M., R.G. and R.G.-O. analyzed the 16S amplicon sequencing data. K.W.-M., J.Y., P.S.-L., H.N. and S.C.S. designed the mass spectrometry experiments. J.Y. performed the experiments. S.C.S and H.N. developed the protocol to detect flg22 peptide and S.C.S analyzed the data. A.E. and N.G. phenotyped the growth of *pWER::FLS2-GFP* transgenic line in natural soil. K.W.-M., Y.N., R.G.-O. and P.S.-L. wrote the manuscript with input from all co-authors. K.W.-M., Y.N. and Y.J. contributed equally to this work.

**Corresponding authors**

Correspondence should be addressed to R.G.-O. and P.S.-L..

## Materials

*Arabidopsis thaliana* ecotype Columbia (Col-0, CS60000), *pepr1pepr2* were lab stocks. *myb15*[39] (SALK_151976) was a gift from Nicole Clay (Yale University, USA). The transgenic line *pWER::FLS2-GFP*[24] (*fls2*: SAIL691_C04 background) was provided by Niko Geldner (Université de Lausanne, Switzerland). flg22 (QRLSTGSRINSAKDDAAGLQIA) and *At*pep1 (ATKVKAKQRGKEKVSSGRPGQHN) peptides were synthesized by EZbiolab.

## Growth Conditions for Plants

*Arabidopsis* seeds were surface-sterilized in 70% ethanol twice for 5 min each followed by a brief wash with 100% ethanol. Seeds were then washed three times with sterile water. Cold-stratified seeds were sowed on agar plates (1%, Difco Agar Granulated, BD Biosciences, discontinued) or Bacto agar (BD Biosciences) prepared with half-strength Murashige and Skoog (MS) medium (Duchefa) and 0.1g/L 2-(*N*-morpholino)ethanesulfonic acid (MES, pH 5.7). Sugars were not provided as additional carbon source unless otherwise specified. Plants were grown under short-day conditions (10 hr light, 14 hr dark) at 21°C/19°C cycle, 65% relative humidity and light intensity of 120 mE $m^{-2}$ $sec^{-1}$. For experiment involving *myb15-1*, surfaced sterilized seeds were sowed on half-strength MS agar plates supplemented with 5g/L sucrose.

## Culture condition for bacteria

Information on individual strains used can be found on *At*-RSPHERE (http://www.at-sphere.com/)[19]. OTU5(p5.e6)[40] was kindly provided by Detlef Weigel (Max Planck Institute for Developmental Biology, Tübingen, Germany). Bacterial strains were prepared by taking an aliquot from the glycerol stock, followed by incubation on 50% tryptic soy broth (TSB) agar plate (Sigma-Aldrich, USA) at 25 °C from one to four days. Before the start of the experiments, strains were cultured in 50% TSB medium to saturation and subcultured to log phase with fresh medium in a 1:5 ratio. Bacterial culture was pelleted by centrifugation at 8k g for 5 min, followed by two washes with 10mM $MgSO_4$.

## Screening for RGI suppressive strains in monoassociation

After washing, bacteria were diluted with 10mM $MgSO_4$ to a concentration of $OD_{600}$ about 0.1. A total 150 µL bacteria suspension was added to still warm 50ml half strength MS agar medium at a final bacterial concentration $OD_{600}$= 0.0005. A final concentration of 1 µM flg22 was added accordingly. Plates were dried for 2 hours before approximately 15 surface-sterilized *pWER::FLS2-GFP* seeds were sowed on each plate. The expression of the flg22 receptor FLS2 in *pWER::FLS2-GFP* is

limited to the root epidermis such that potential inter-organ shoot-to-root signal upon flg22 perception is minimized. Plates were sealed with 3M tape and transferred to the phytochamber for incubation. One week after germination, plants with delayed germination were removed and the plates were trimmed to about 10 plants remaining. Pictures were taken 3 weeks after incubation and the primary root lengths were quantified by ImageJ. Shoots were separated from the roots and fresh shoot weight of individual plant was taken. For experiments using 1 µM *At*pep1, wild-type Col-0 plants were used instead.

A phylogenetic tree of selected strains from *At*-RSPHERE was performed previously[19] and visualized by iTOL[51]. Those strains leading to a rescue of RGI with root length longer than 2cm (average root length of germ-free flg22-treated *pWER::FLS2-GFP* plants=1.53cm; n=37) upon coinoculation with 1 µM flg22 and exhibited consistent suppressive activity across two biological replicates were considered as "suppressive". Suppressive strains were indicated with a red triangle in figure 1a. For the inoculation of SynCom, each bacterium was inoculated to a final concentration of $OD_{600}$= 0.0005, i.e. for a 5-member SynCom, the total bacteria added was $OD_{600}$=0.0025. The 5-member SynCom is composed of Actinobacteria, Alpha-, Beta- and Gamma-proteobacteria. Bacteriodetes and Firmicutes were not included in these SynCom since no strains with differential ability to suppress RGI were identified in these two phyla. Composition of SynCom used in this manuscript can be found in Table S1.

**_16S_ amplicon sequencing and community profiling**

For *16S* community profiling, root samples were harvested and libraries were processed according to previously published protocol [4]. Briefly, plants were germinated with the indicated SynCom in the presence or absence of 1 µM flg22 and incubated for 14 days before harvesting. Plants were inoculated with SynCom NS1 and S1 for experiment 1 (Fig 2a,d and Extended Data Fig. 5a,d); SynCom NS3 and S3 for experiment 2 (Fig 2b,e and Extended Data Fig. 5b,e); and SynCom NS4 and S2 for experiment 3 (Fig 2c,f and Extended Data Fig. 5c,f). Plant roots were separated from the shoots and pooled from three plates from each biological replicate. Roots were washed briefly with sterile water and blotted dry before being transferred into Lysing Matrix E tubes (MP Biomedicals) at -80˚C until processing. Samples were homogenized using Precellys 24 homogenizer (6200rpm 2X30 sec, 15 sec pauses in between; Bertin Technologies, Netherlands). Total root DNA was extracted using the FastDNA SPIN Kit for Soil (MP Biomedicals) according to the manufacturer's instructions, eluted in 80 µl elution buffer and quantified using Quant-iT PicoGreen dsDNA Assay (ThermoFisher). Samples were diluted to 3.5 ng/µl and 3 µL samples were used in a three-step PCR amplification protocol.

Step 1: the V5–V7 region of the bacterial 16S rRNA gene was amplified in triplicate reactions with primers 799F and 1192R in a 25 µL reaction volume containing 2 U DFS-Taq DNA polymerase (Bioron), 1× incomplete buffer, 2 mM MgCl2, 0.3% bovine serum albumin, 0.2 mM dNTPs (Life Technologies) and 0.3 µM forward and reverse primers. The same PCR parameters were used for each primer pair (94 °C for 2 min, 94 °C for 30 s, 55 °C for 30 s, 72 °C for 30 s and 72 °C for 10 min for 25 cycles). Primers and proteins were digested by adding 1 µl of Antarctic phosphatase, 1 µl Exonuclease I and 2.44 µl Antarctic Phosphatase buffer (New England Biolabs) to 20 µl of the pooled replicate reactions at 37 °C for 30 min, followed by enzyme deactivation at 85 °C for 15 min. Reactions were centrifuged for 15 min at 4000 rpm and 3 µl of supernatant were used for the second PCR step in triplicate reactions.

Step 2: PCR reactions were performed as stated above with the number of cycles reduced to ten using primer pairs 799F and individual reverse barcoded primers. PCR quality and quantity were estimated by loading 5 µl of each reaction on a 1.5% agarose gel. Approximately similar amount of DNA of samples from the same biological replicate were pooled and the mixtures were loaded on a 1.5% agarose gel. DNA bands with the correct size were cut out and purified using the QIAquick Gel Extraction Kit (Qiagen).

Step 3: Gel-purified DNA were used as templates for the third PCR using forward barcoded primers and p7_pad_R with a total of ten cycles. PCR reactions were loaded on a 1.5% agarose gel and DNA bands with the correct size were cut out and purified using the QIAquick Gel Extraction Kit (Qiagen). Double-barcoded DNA was purified and concentrated by Agencourt AMPure XP beads. Concentration of the purified DNA was determined using Quant-iT PicoGreen dsDNA Assay (ThermoFisher). Paired-end Illumina sequencing was performed using 20ng/ul final library in house using the MiSeq sequencer and custom sequencing primers.

**Amplicon data analysis**

Forward and reverse sequencing reads were denoised and demultiplexed separately according to the barcode sequence using QIIME[52] with the following parameters: *phred*=30; *bc_err*=2. After quality-filtering, merging of paired-end reads, amplicon tags were then aligned to a reference set of sequences obtained from the whole-genome assemblies of every strain included in each experiment by using USEARCH (*uparse_ref* command)[53]. A count feature table for each strain was generated by using only perfect matches to the reference sequence from the genome collection. This count table was employed for subsequent diversity and enrichment analyses. Alpha and beta diversities were calculated after normalizing count tables by the total number of reads per sample. The Simpson

index was obtained using the *diversity* function in vegan package. Bray-Curtis dissimilarity index was calculated using the *vegdist* function in the vegan package[54] and used for unconstrained ordination by Principal Coordinate Analysis (PCoA). All data were used except for biological replicate c of experiment 1 due to potential contamination issue or PCR error. Constrained PCoA (CPCoA) was performed with the vegan *capscale* function on the Bray-Curtis dissimilarity matrices constraining by the interaction between flg22 treatment and SynCom variables and conditioning by technical parameters. Statistical significance of separation between community profiles according to flg22 treatment was determined using PERMANOVA with 999 permutations (*anova.cca* function in vegan). Finally, all amplicon data was visualized using the *ggplot2* [55] R package.

**Preparation of cell-free supernatant of bacteria**

15 to 20 Col-0 were pregerminated on half strength MS agar plate supplemented with 5g/L sucrose. After two weeks, 20ml washed bacterial suspension ($OD_{600}$=0.0005) in half strength MS medium without sucrose was added to each plate. After another seven days of coincubation, fresh half strength MS medium was added to obtain a final 20ml supernatant after 1 hour of gentle shaking. The supernatant was filter-sterilized by passing through 0.22um PES filter (Millipore). The filtrates were separated into two fractions by passing through the 3kDa ultracentrifugal filter (4000rpm, 60min, Amicon Millipore). The filtrates were filter-sterilized by passing through the 0.22um filter again if necessary. Finally, the fraction larger than 3kDa was heat inactivated by boiling for 5 minutes. To test for RGI suppressive activity, surface sterilized seeds were germinated in 1 ml supernatant supplemented with 5g/L sucrose and 1 µM *At*pep1 or flg22 in a 12-well plate for two weeks.

**Generation of *ΔhrcC* mutant of *Pseudomonas* strain 569**

569 deletion mutant was generated *via* homologous recombination protocol[56]. Briefly, PCR fragments flanking the upstream and downstream region of *hrcC* gene was PCR amplified and cloned into *pK18mobsacB*. The FRT-flanked cassette from *pCPP5209* was inserted between the two hrcC fragments. The resultant *pK18mobsacB::ΔhrcC* construct was electroporated into log-phase grown 569 prewashed and resuspended in 0.3M sucrose at 2.5kV and 150 ohm by a Biorad electroporator. The transformant was selected on half TSB plate supplemented with 25ng/µL Gentamycin. The double-crossover deletion mutant was further confirmed by colony PCR and Sanger sequencing.

**Mass spectrometry**

For *in vitro* detection of flg22, 1 µM flg22 was co-incubated with 1ml supernatant for 1 hour at room temperature. Half strength MS medium without sugar was used as a control. 100 µL aliquots sample

were mixed with 200 µL UA (8M urea in 100 mM Tris-HCl pH 8.5) and adjusted to 10 mM Dithiothreitol (DTT) using 1M stock. Samples were loaded onto 30 kD spin filters (Vivacon 500, Sartorius) and centrifuged at 14k g for 15 min. The filtrate was collected and loaded onto 2 kD spin filters (Vivacon 500, Sartorius) and centrifuged at 14k g for 30 min, after which 300 µL UA were added and samples were centrifuged again (14k g, 45 min, or until most liquid had passed through the filter). Next, 100 µL 55 mM chloroacetamide were added to the filter and samples were incubated for 30 min in the dark, after which they were centrifuged at 14k g for 20 min. 300 µL UA were added and samples were centrifuged at 14k g for 45 min. Samples were washed twice with 300 µL 100mM Tris-HCl, pH 8.5, by centrifugation (14k g, 45 min). For elution, 200 µL Tris-HCl were added, and the inverted spin filters were centrifuged at 2k g for 2 min to collect eluate into a fresh tube. The eluates were desalted using StageTips with C18 Empore disk membranes (3 M)[57], final elution was performed using 40% acetonitrile, 0.1% TFA. Samples were dried in a vacuum evaporator, and dissolved in 10 µL 2% acetonitrile (ACN), 0.1% trifluoroacetic acid (TFA) for analysis.

**LC-MS/MS data acquisition and data analysis.** Samples were analyzed using an EASY-nLC 1000 (Thermo Fisher) coupled to a QExactive mass spectrometer (Thermo Fisher). Peptides were separated on 16 cm frit-less silica emitters (New Objective, 0.75 µm inner diameter), packed in-house with reversed-phase ReproSil-Pur C18 AQ 3 µm resin (Dr. Maisch). Peptides were loaded on the column and eluted for 50 min using a segmented linear gradient of 5% to 95% solvent B (0 min : 5%B; 0-5 min -> 5%B; 5-25 min -> 20%B; 25-35 min ->35%B; 35-40 min -> 95%B; 40-50 min ->95%B) (solvent A 0% ACN, 0.1% formic acid (FA); solvent B 80% ACN, 0.1% FA) at a flow rate of 300 nL/min. Mass spectra were acquired in data-dependent acquisition mode with a TOP10 method. MS spectra were acquired in the Orbitrap analyzer with a mass range of 300–1500 m/z at a resolution of 70,000 FWHM and a target value of $3\times10^6$ ions. Precursors were selected with an isolation window of 2.0 m/z. HCD fragmentation was performed at a normalized collision energy of 25. MS/MS spectra were acquired with a target value of $5x10^5$ ions at a resolution of 17,500 FWHM, a maximum injection time of 85 ms and a fixed first mass of m/z 100. Peptides with a charge of 1, greater than 6, or with unassigned charge state were excluded from fragmentation for $MS^2$, dynamic exclusion for 20s prevented repeated selection of precursors.

Raw data was directly analyzed on MS1 level using Skyline (https://skyline.ms)[58] against the sequence of the flg22 peptide. LysC specificity was required and a maximum of two missed cleavages allowed. Minimal peptide length was set to seven maximum length to 25 amino acids. Carbamidomethylation of cysteine, oxidation of methionine and protein N-terminal acetylation were set as modifications. Results were filtered for precursor charges of 2, 3. Peaks of the intact flg22 peptide precursor were integrated manually, peak areas were exported for further processing.

**Infection experiments**

Plants were pre-germinated on half strength MS agar plate inoculated with the indicated SynCom for 14 days. Plants were then flood inoculated with a bacterial suspension *of Pseudomonas* strain 401 or OTU5 (p5. e6) ($O.D._{600}$=0.0001) in 10mM $MgSO_4$ supplemented with 0.005% silwet. Excessive liquid was removed five minutes after flood inoculation and plants were transferred to a new half strength MS agar for further incubation. After 1 or 2 days, shoots and roots were separated, roots and shoots from five and three individual plants were pooled together after brief washing and blotted dry with sterile filter paper. Samples were homogenized with metal beads in 500ul $MgSO_4$ using Precellys 24 homogenizer (6200 rpm 2X30 sec, 15 sec pauses in between; Bertin Technologies, Netherlands). *Pseudomonas* strain 401 and OTU5 (p5. e6) were transformed with *pBBR1-MCS5* carrying a gentamycin resistant cassette. Serial dilution was performed and bacterial dilutions were spread on 50% TSB plates supplemented with 25ng/µL Gentamycin to select for the strain of interest until single colonies appeared.

***In vitro* halo-of-inhibition assay**

100 µL washed *Pseudomonas* strain 401 was inoculated into 50ml warm 25% TSB medium with an initial $OD_{600}$=0.1. After solidification, 10 µL pre-washed bacterial suspension prepared from 1ml saturated overnight bacterial culture from individual strains was spotted on the 401-preinoculated plates. Any halo-of-inhibition was recorded up to 5 days after incubation at 25 °C.

**Transcriptome experiments**

Plants were germinated with the indicated SynCom in the presence or absence of 1 µM flg22 and incubated for 14 days before harvesting. For transcriptome experiments, Col-0 plants were inoculated with SynCom NS3 and SynCom S3 (Fig. 3); *pWER::FLS2-GFP* plants were inoculated with SynCom NS1 and SynCom S1 (Extended Data Fig. 6). For transcriptome experiments, plants were not transferred to minimize induced damage. Roots from three plates (minimum 15 plants) were combined as one replicate and a total of three replicates were sampled for each condition. Roots were washed briefly with sterile water and blotted dry before being transferred into Lysing Matrix E tubes (MP Biomedicals) at -80˚C until processing. Roots were homogenized with Lysing Matrix E using prechilled adapter and TissueLyser II (Qiagen, 20/sec, 1 minute). RNA was extracted with the Plant RNeasy Mini Kit (Qiagen) according to the manufacturer's instructions. RNA quality was determined using a 2100 Bioanalyzer (Agilent Technologies, USA). Preparation of Illumina sequencing libraries was conducted by the Max Planck Genome Center) using an input of 1µg total RNA. Sequences were

generated using the Illumina HiSeq2500 platform. Approximately 6 M paired-end reads and 20 M single-end reads per sample with a length of 150 bp were generated for Col-0 and *pWER::FLS2-GFP* based experiments.

**RNA-Seq data analysis**

Raw Illumina RNA-Seq reads were pre-processed using fastp (v0.19.10)[59] with default settings for paired-end (Col-0 experiment) or single-end reads (*pWER::FLS2-GFP* experiment). For single-end reads, low quality sequences from the head (8 bases) and tail (2 bases) were trimmed. High quality reads were pseudo-aligned to TAIR 10 *Arabidopsis thaliana* transcriptome reference (Ensembl)[60] using kallisto (v0.46.1)[61]. On average, 6.7 million paired-end and 18.1 million single-end reads per sample were mapped to the reference *Arabidopsis* transcriptome, respectively. After removal of low abundant transcripts that were absent in at least two replicates under each condition, count data were imported using the *tximport* [62] package.

Differential expression analyses were performed using the *DESeq2*[63] package. Firstly, raw counts were normalized with respect to the library size (*rlog* function) and $\log_2$ transformed. We tested for sample batch effects by surrogate variable (SV) analysis using the *sva*[64] package. Significant SVs were automatically detected and integrated into the model for differential analyses. Principal component analysis (*prcomp* function) based on whole transcripts were performed and plotted to visualize the cluster and variance of biological replicates under each condition. Abundance of *Arabidopsis* latent virus-1 reads did not correlate with sample variances and therefore removed from downstream analyses. Pair-wise comparisons were designed as: (1) flg22 treatment effect only, (2) non-suppressive and suppressive SynCom effect only, (3) flg22 treatment plus SynCom effects, (4) living *vs.* heat-killed bacteria. Transcripts with fold-changes > 1.5 and adjusted *p*-value for multiple comparisons (Benjamini–Hochberg method) equal to or below 0.05 were considered significant.

The $\log_2$ scaled counts were normalized by the identified SVs using the *limma*[65] package (*removeBatchEffect* function), and transformed as median-centered *z*-score by transcripts (scaled counts, *scale* function). Then *z*-scores were used to conduct *k*-means clustering for all transcripts. The cluster number ($k$ = 10) was determined by sum of squared error and Akaike information criterion. Next, confirmed transcripts with similar expression patterns were grouped in the same cluster. Differentially expressed transcripts (3,718 in *pWER::FLS2-GFP* and 4,450 in Col-0 experiments) and cluster results were visualized using heatmaps generated by *ComplexHeatmap*[66] package.

Gene ontology (GO) enrichment for each cluster using the whole *Arabidopsis* transcriptome as background were performed with the *goseq*[67] package with the consideration of transcripts length. GO annotations were retrieved from the Gene Ontology Consortium[68,69] (September 2019). Significantly changed biological process GO terms (adjusted *p*-value < 0.05) were visualized in dot plots using the *clusterProfiler*[70] package. Defense-related genes were extracted based on the GO-terms annotation with manual curation. These genes were marked in Table S3 and Table S4.

A GO-gene network was built by connecting GO terms with shared differentially changed genes (Jaccard similarity > 0.2), so that GO terms holding close function annotations were gathered. Nodes in the network were colored according to their representation in the *k*-means clustering analysis, while their size corresponded to the number of genes annotated in the corresponding GO term. GO-gene networks were visualized in Cytoscape[71] with a modified configuration from metascape[72].

Differentially expressed genes from another two RNA-Seq data sets Teixeira *et al.,* 2020 and Harbort and Hashimoto *et al.* 2020 were used to confirm genes involved in SynCom response. The RNA-Seq analyses pipeline was the same as describe above. GO enrichment were conducted based on the common significantly changed genes from this study and published data sets using *clusterProfiler* package.

**Quantitative real time PCR**

Roots from at least five 2-week-old plants were pooled and total RNA was extracted using the RNeasy Plant Mini Kit (Qiagen, Germany) according to the manufacturer's instructions. 200-500ng total RNA was DNase treated followed by 1$^{st}$ strand cDNA synthesis using oligo dT primers and superscript II reverse transcriptase (Invitrogen). cDNA was diluted 10 times and 5 µL sample was used as a template for quantitative PCR analysis in a 20 µL reaction mixture supplemented with 1X iQ SYBR Green (Bio-Rad, USA), and 0.2 µM primer each. *UBQ5* was used for internal normalization. Primers used in this study can be found in Table S5.

**Statistical analysis**

Analyses were performed using the R environment. *t*-test, Dunn's Kruskal-Wallis, Dunnett's test and ANOVA were used to test for statistical significance. A *p*-value smaller than 0.05 was considered significant.

**Data and software availability**

Raw transcriptome and *16S* rRNA amplicon sequencing data from this project were deposited at the EBI Sequence Read Archive under the accession number GSE157128. Mass spectrometry data has been deposited to Panorama Public (https://panoramaweb.org/flg22_RGI.url) and ProteomeExchange (PDX020452). We also make all data and scripts available to the reviewers and the editorial office at https://github.com/YulongNiu/MPIPZ_microbe-host_homeostasis.

References


1 Hassani, M. A., Duran, P. & Hacquard, S. Microbial interactions within the plant holobiont. *Microbiome* **6**, 58, doi:10.1186/s40168-018-0445-0 (2018).

2 Lundberg, D. S. *et al.* Defining the core Arabidopsis thaliana root microbiome. *Nature* **488**, 86-90, doi:10.1038/nature11237 (2012).

3 Schlaeppi, K., Dombrowski, N., Oter, R. G., Ver Loren van Themaat, E. & Schulze-Lefert, P. Quantitative divergence of the bacterial root microbiota in Arabidopsis thaliana relatives. *Proc Natl Acad Sci U S A* **111**, 585-592, doi:10.1073/pnas.1321597111 (2014).

4 Bulgarelli, D. *et al.* Revealing structure and assembly cues for Arabidopsis root-inhabiting bacterial microbiota. *Nature* **488**, 91-95, doi:10.1038/nature11336 (2012).

5 Thiergart, T. *et al.* Root microbiota assembly and adaptive differentiation among European Arabidopsis populations. *Nat Ecol Evol* **4**, 122-131, doi:10.1038/s41559-019-1063-3 (2020).

6 Jacoby, R., Peukert, M., Succurro, A., Koprivova, A. & Kopriva, S. The Role of Soil Microorganisms in Plant Mineral Nutrition-Current Knowledge and Future Directions. *Front Plant Sci* **8**, 1617, doi:10.3389/fpls.2017.01617 (2017).

7 Bulgarelli, D., Schlaeppi, K., Spaepen, S., Ver Loren van Themaat, E. & Schulze-Lefert, P. Structure and functions of the bacterial microbiota of plants. *Annu Rev Plant Biol* **64**, 807-838, doi:10.1146/annurev-arplant-050312-120106 (2013).

8 Huang, A. C. *et al.* A specialized metabolic network selectively modulates Arabidopsis root microbiota. *Science* **364**, doi:10.1126/science.aau6389 (2019).

9 Koprivova, A. *et al.* Root-specific camalexin biosynthesis controls the plant growth-promoting effects of multiple bacterial strains. *Proc Natl Acad Sci U S A* **116**, 15735-15744, doi:10.1073/pnas.1818604116 (2019).

10 Lebeis, S. L. *et al.* PLANT MICROBIOME. Salicylic acid modulates colonization of the root microbiome by specific bacterial taxa. *Science* **349**, 860-864, doi:10.1126/science.aaa8764 (2015).

11 Hu, L. *et al.* Root exudate metabolites drive plant-soil feedbacks on growth and defense by shaping the rhizosphere microbiota. *Nat Commun* **9**, 2738, doi:10.1038/s41467-018-05122-7 (2018).

12 Castrillo, G. *et al.* Root microbiota drive direct integration of phosphate stress and immunity. *Nature* **543**, 513-518, doi:10.1038/nature21417 (2017).

13 Stringlis, I. A. *et al.* Root transcriptional dynamics induced by beneficial rhizobacteria and microbial immune elicitors reveal signatures of adaptation to mutualists. *Plant J* **93**, 166-180, doi:10.1111/tpj.13741 (2018).

14 Saijo, Y., Loo, E. P. & Yasuda, S. Pattern recognition receptors and signaling in plant-microbe interactions. *Plant J* **93**, 592-613, doi:10.1111/tpj.13808 (2018).

15 Wan, W. L., Frohlich, K., Pruitt, R. N., Nurnberger, T. & Zhang, L. Plant cell surface immune receptor complex signaling. *Curr Opin Plant Biol* **50**, 18-28, doi:10.1016/j.pbi.2019.02.001 (2019).

16 Zipfel, C. *et al.* Bacterial disease resistance in Arabidopsis through flagellin perception. *Nature* **428**, 764-767, doi:10.1038/nature02485 (2004).

17 Huot, B., Yao, J., Montgomery, B. L. & He, S. Y. Growth-defense tradeoffs in plants: a balancing act to optimize fitness. *Mol Plant* **7**, 1267-1287, doi:10.1093/mp/ssu049 (2014).

18 Jones, J. D. & Dangl, J. L. The plant immune system. *Nature* **444**, 323-329, doi:10.1038/nature05286 (2006).

19 Bai, Y. *et al.* Functional overlap of the Arabidopsis leaf and root microbiota. *Nature* **528**, 364-369, doi:10.1038/nature16192 (2015).

20 Garrido-Oter, R. *et al.* Modular Traits of the Rhizobiales Root Microbiota and Their Evolutionary Relationship with Symbiotic Rhizobia. *Cell Host Microbe* **24**, 155-167 e155, doi:10.1016/j.chom.2018.06.006 (2018).

21 Yu, K. *et al.* Rhizosphere-Associated Pseudomonas Suppress Local Root Immune Responses by Gluconic Acid-Mediated Lowering of Environmental pH. *Curr Biol* **29**, 3913-3920 e3914, doi:10.1016/j.cub.2019.09.015 (2019).

22 Hacquard, S., Spaepen, S., Garrido-Oter, R. & Schulze-Lefert, P. Interplay Between Innate Immunity and the Plant Microbiota. *Annu Rev Phytopathol* **55**, 565-589, doi:10.1146/annurev-phyto-080516-035623 (2017).

23 Teixeira, P. J. P., Colaianni, N. R., Fitzpatrick, C. R. & Dangl, J. L. Beyond pathogens: microbiota interactions with the plant immune system. *Curr Opin Microbiol* **49**, 7-17, doi:10.1016/j.mib.2019.08.003 (2019).

24 Wyrsch, I., Dominguez-Ferreras, A., Geldner, N. & Boller, T. Tissue-specific FLAGELLIN-SENSING 2 (FLS2) expression in roots restores immune responses in Arabidopsis fls2 mutants. *New Phytol* **206**, 774-784, doi:10.1111/nph.13280 (2015).

25 Emonet, A. *et al.* Spatially Restricted Immune Responses Allow for Root Meristematic Activity During Bacterial Colonisation. 2020.2008.2003.233817, doi:10.1101/2020.08.03.233817 %J bioRxiv (2020).

26 Poncini, L. *et al.* In roots of Arabidopsis thaliana, the damage-associated molecular pattern AtPep1 is a stronger elicitor of immune signalling than flg22 or the chitin heptamer. *PLoS One* **12**, e0185808, doi:10.1371/journal.pone.0185808 (2017).

27 Finkel, O. M. *et al.* A single bacterial genus maintains root development in a complex microbiome. 645655, doi:10.1101/645655 %J bioRxiv (2020).

28 Pel, M. J. *et al.* Pseudomonas syringae evades host immunity by degrading flagellin monomers with alkaline protease AprA. *Mol Plant Microbe Interact* **27**, 603-610, doi:10.1094/MPMI-02-14-0032-R (2014).

29 Harbort, C. J., Hashimoto, M., Inoue, H., Niu, Y., Guan, R., Rombolà, A.D., Kopriva, S, Voges, M. J. E. E. E., Sattely, E. S., Garrido-Oter, R., Schulze-Lefert, P. Root-secreted coumarins and the microbiota interact to improve iron nutrition in Arabidopsis. *Cell Host Microbe* **in press** (2020).

30 Frerigmann, H., Glawischnig, E. & Gigolashvili, T. The role of MYB34, MYB51 and MYB122 in the regulation of camalexin biosynthesis in Arabidopsis thaliana. *Front Plant Sci* **6**, 654, doi:10.3389/fpls.2015.00654 (2015).

31 Frerigmann, H. *et al.* Regulation of Pathogen-Triggered Tryptophan Metabolism in Arabidopsis thaliana by MYB Transcription Factors and Indole Glucosinolate Conversion Products. *Mol Plant* **9**, 682-695, doi:10.1016/j.molp.2016.01.006 (2016).

32 Zhang, Y. *et al.* Control of salicylic acid synthesis and systemic acquired resistance by two members of a plant-specific family of transcription factors. *Proc Natl Acad Sci U S A* **107**, 18220-18225, doi:10.1073/pnas.1005225107 (2010).

33 Hartmann, M. *et al.* Flavin Monooxygenase-Generated N-Hydroxypipecolic Acid Is a Critical Element of Plant Systemic Immunity. *Cell* **173**, 456-469 e416, doi:10.1016/j.cell.2018.02.049 (2018).

34 Hou, S. *et al.* The secreted peptide PIP1 amplifies immunity through receptor-like kinase 7. *PLoS Pathog* **10**, e1004331, doi:10.1371/journal.ppat.1004331 (2014).

35 Zhou, F. *et al.* Co-incidence of Damage and Microbial Patterns Controls Localized Immune Responses in Roots. *Cell* **180**, 440-453 e418, doi:10.1016/j.cell.2020.01.013 (2020).

36 Millet, Y. A. *et al.* Innate immune responses activated in Arabidopsis roots by microbe-associated molecular patterns. *Plant Cell* **22**, 973-990, doi:10.1105/tpc.109.069658 (2010).

37 Zhao, L. *et al.* KLU suppresses megasporocyte cell fate through SWR1-mediated activation of WRKY28 expression in Arabidopsis. *Proc Natl Acad Sci U S A* **115**, E526-E535, doi:10.1073/pnas.1716054115 (2018).

38 Zou, L. *et al.* Transcription factor WRKY30 mediates resistance to Cucumber mosaic virus in Arabidopsis. *Biochem Biophys Res Commun* **517**, 118-124, doi:10.1016/j.bbrc.2019.07.030 (2019).

39 Chezem, W. R., Memon, A., Li, F. S., Weng, J. K. & Clay, N. K. SG2-Type R2R3-MYB Transcription Factor MYB15 Controls Defense-Induced Lignification and Basal Immunity in Arabidopsis. *Plant Cell* **29**, 1907-1926, doi:10.1105/tpc.16.00954 (2017).

40 Karasov, T. L. *et al.* Arabidopsis thaliana and Pseudomonas Pathogens Exhibit Stable Associations over Evolutionary Timescales. *Cell Host Microbe* **24**, 168-179 e164, doi:10.1016/j.chom.2018.06.011 (2018).

41 Karasov, T. L. *et al.* The relationship between microbial biomass and disease in the Arabidopsis thaliana phyllosphere. 828814, doi:10.1101/828814 %J bioRxiv (2019).

42 Edwards, J. *et al.* Structure, variation, and assembly of the root-associated microbiomes of rice. *Proc Natl Acad Sci U S A* **112**, E911-920, doi:10.1073/pnas.1414592112 (2015).

43 Zamioudis, C., Mastranesti, P., Dhonukshe, P., Blilou, I. & Pieterse, C. M. Unraveling root developmental programs initiated by beneficial Pseudomonas spp. bacteria. *Plant Physiol* **162**, 304-318, doi:10.1104/pp.112.212597 (2013).

44 Lopez-Bucio, J. *et al.* Bacillus megaterium rhizobacteria promote growth and alter root-system architecture through an auxin- and ethylene-independent signaling mechanism in Arabidopsis thaliana. *Mol Plant Microbe Interact* **20**, 207-217, doi:10.1094/MPMI-20-2-0207 (2007).

45 Hernandez, M., Dumont, M. G., Yuan, Q. & Conrad, R. Different bacterial populations associated with the roots and rhizosphere of rice incorporate plant-derived carbon. *Appl Environ Microbiol* **81**, 2244-2253, doi:10.1128/AEM.03209-14 (2015).

46 Alden, L., Demoling, F. & Baath, E. Rapid method of determining factors limiting bacterial growth in soil. *Appl Environ Microbiol* **67**, 1830-1838, doi:10.1128/AEM.67.4.1830-1838.2001 (2001).

47 Levy, A. *et al.* Genomic features of bacterial adaptation to plants. *Nat Genet* **50**, 138-150, doi:10.1038/s41588-017-0012-9 (2017).

48 Saleem, M., Hu, J. & Jousset, A. More Than the Sum of Its Parts: Microbiome Biodiversity as a Driver of Plant Growth and Soil Health. *Annu Rev Ecol Evol S* **50**, 145-+, doi:10.1146/annurev-ecolsys-110617-062605 (2019).

49 Chen, T. *et al.* A plant genetic network for preventing dysbiosis in the phyllosphere. *Nature* **580**, 653-657, doi:10.1038/s41586-020-2185-0 (2020).

50 de Zelicourt, A. *et al.* Ethylene induced plant stress tolerance by Enterobacter sp. SA187 is mediated by 2-keto-4-methylthiobutyric acid production. *PLoS Genet* **14**, e1007273, doi:10.1371/journal.pgen.1007273 (2018).

51 Letunic, I. & Bork, P. Interactive Tree Of Life (iTOL) v4: recent updates and new developments. *Nucleic Acids Res* **47**, W256-W259, doi:10.1093/nar/gkz239 (2019).

52 Caporaso, J. G. *et al.* QIIME allows analysis of high-throughput community sequencing data. *Nat Methods* **7**, 335-336, doi:10.1038/nmeth.f.303 (2010).

53 Edgar, R. C. Search and clustering orders of magnitude faster than BLAST. *Bioinformatics* **26**, 2460-2461, doi:10.1093/bioinformatics/btq461 (2010).

54 Oksanen, J. *et al.* vegan: Community Ecology Package. R package version 2.4-3. (2016).

55 Wickham, H., Sievert, C. & Springer International, P. *ggplot2 : elegant graphics for data analysis*. (2016).

56 Kvitko, B. H. & Collmer, A. Construction of Pseudomonas syringae pv. tomato DC3000 mutant and polymutant strains. *Methods Mol Biol* **712**, 109-128, doi:10.1007/978-1-61737-998-7_10 (2011).

57 Rappsilber, J., Ishihama, Y. & Mann, M. Stop and go extraction tips for matrix-assisted laser desorption/ionization, nanoelectrospray, and LC/MS sample pretreatment in proteomics. *Anal Chem* **75**, 663-670, doi:10.1021/ac026117i (2003).

58 MacLean, B. *et al.* Skyline: an open source document editor for creating and analyzing targeted proteomics experiments. *Bioinformatics* **26**, 966-968, doi:10.1093/bioinformatics/btq054 (2010).

59 Chen, S., Zhou, Y., Chen, Y. & Gu, J. fastp: an ultra-fast all-in-one FASTQ preprocessor. *Bioinformatics* **34**, i884-i890, doi:10.1093/bioinformatics/bty560 (2018).
60 Yates, A. D. *et al.* Ensembl 2020. *Nucleic Acids Res* **48**, D682-D688, doi:10.1093/nar/gkz966 (2020).
61 Bray, N. L., Pimentel, H., Melsted, P. & Pachter, L. Near-optimal probabilistic RNA-seq quantification. *Nat Biotechnol* **34**, 525-527, doi:10.1038/nbt.3519 (2016).
62 Soneson, C., Love, M. I. & Robinson, M. D. Differential analyses for RNA-seq: transcript-level estimates improve gene-level inferences. *F1000Res* **4**, 1521, doi:10.12688/f1000research.7563.2 (2015).
63 Love, M. I., Huber, W. & Anders, S. Moderated estimation of fold change and dispersion for RNA-seq data with DESeq2. *Genome Biol* **15**, 550, doi:10.1186/s13059-014-0550-8 (2014).
64 Leek, J. T., Johnson, W. E., Parker, H. S., Jaffe, A. E. & Storey, J. D. The sva package for removing batch effects and other unwanted variation in high-throughput experiments. *Bioinformatics* **28**, 882-883, doi:10.1093/bioinformatics/bts034 (2012).
65 Ritchie, M. E. *et al.* limma powers differential expression analyses for RNA-sequencing and microarray studies. *Nucleic Acids Res* **43**, e47, doi:10.1093/nar/gkv007 (2015).
66 Gu, Z., Eils, R. & Schlesner, M. Complex heatmaps reveal patterns and correlations in multidimensional genomic data. *Bioinformatics* **32**, 2847-2849, doi:10.1093/bioinformatics/btw313 (2016).
67 Young, M. D., Wakefield, M. J., Smyth, G. K. & Oshlack, A. Gene ontology analysis for RNA-seq: accounting for selection bias. *Genome Biol* **11**, R14, doi:10.1186/gb-2010-11-2-r14 (2010).
68 Ashburner, M. *et al.* Gene ontology: tool for the unification of biology. The Gene Ontology Consortium. *Nat Genet* **25**, 25-29, doi:10.1038/75556 (2000).
69 The Gene Ontology, C. The Gene Ontology Resource: 20 years and still GOing strong. *Nucleic Acids Res* **47**, D330-D338, doi:10.1093/nar/gky1055 (2019).
70 Yu, G., Wang, L. G., Han, Y. & He, Q. Y. clusterProfiler: an R package for comparing biological themes among gene clusters. *OMICS* **16**, 284-287, doi:10.1089/omi.2011.0118 (2012).
71 Shannon, P. *et al.* Cytoscape: a software environment for integrated models of biomolecular interaction networks. *Genome Res* **13**, 2498-2504, doi:10.1101/gr.1239303 (2003).
72 Zhou, Y. *et al.* Metascape provides a biologist-oriented resource for the analysis of systems-level datasets. *Nat Commun* **10**, 1523, doi:10.1038/s41467-019-09234-6 (2019).

# Figures

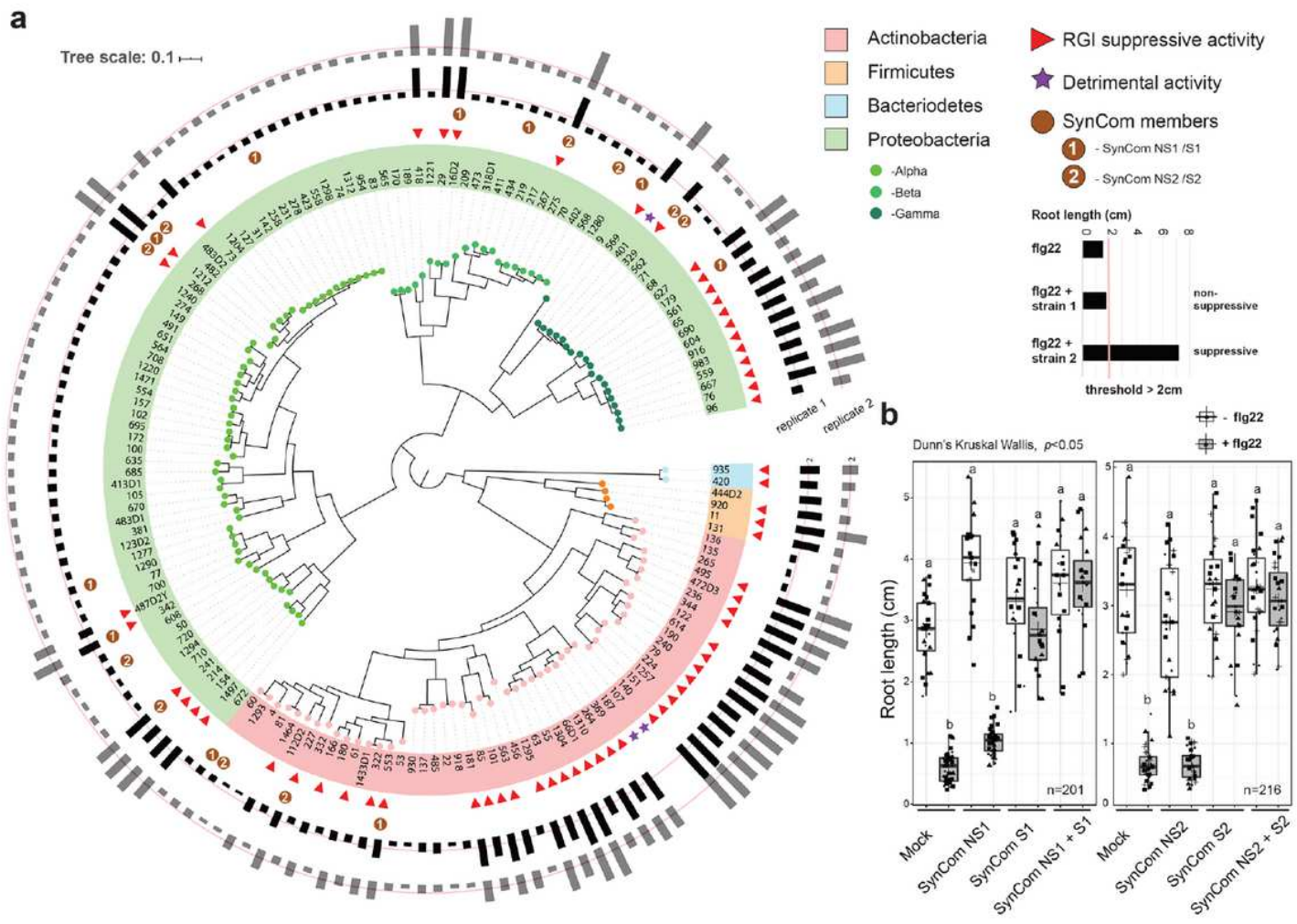


**Figure 1**

At-RSPHERE root commensals exhibit strain-specific variation to suppress flg22-mediated RGI in pWER::FLS2-GFP plants. (a) Phylogenetic tree showing the distribution of strains exhibiting RGI suppressive activity. The outer rings represent root lengths of 3-week old plants treated with 1µM flg22 and individual strains (OD600=0.0005). The threshold for suppressive activity is indicated by the red line i.e. root length > 2cm. (b) The impact of 4 independent 5-member SynComs (Table S1) differential in RGI suppressive activity on flg22-mediated RGI. Shapes correspond to biological replicates. Different letters indicate statistical significance.

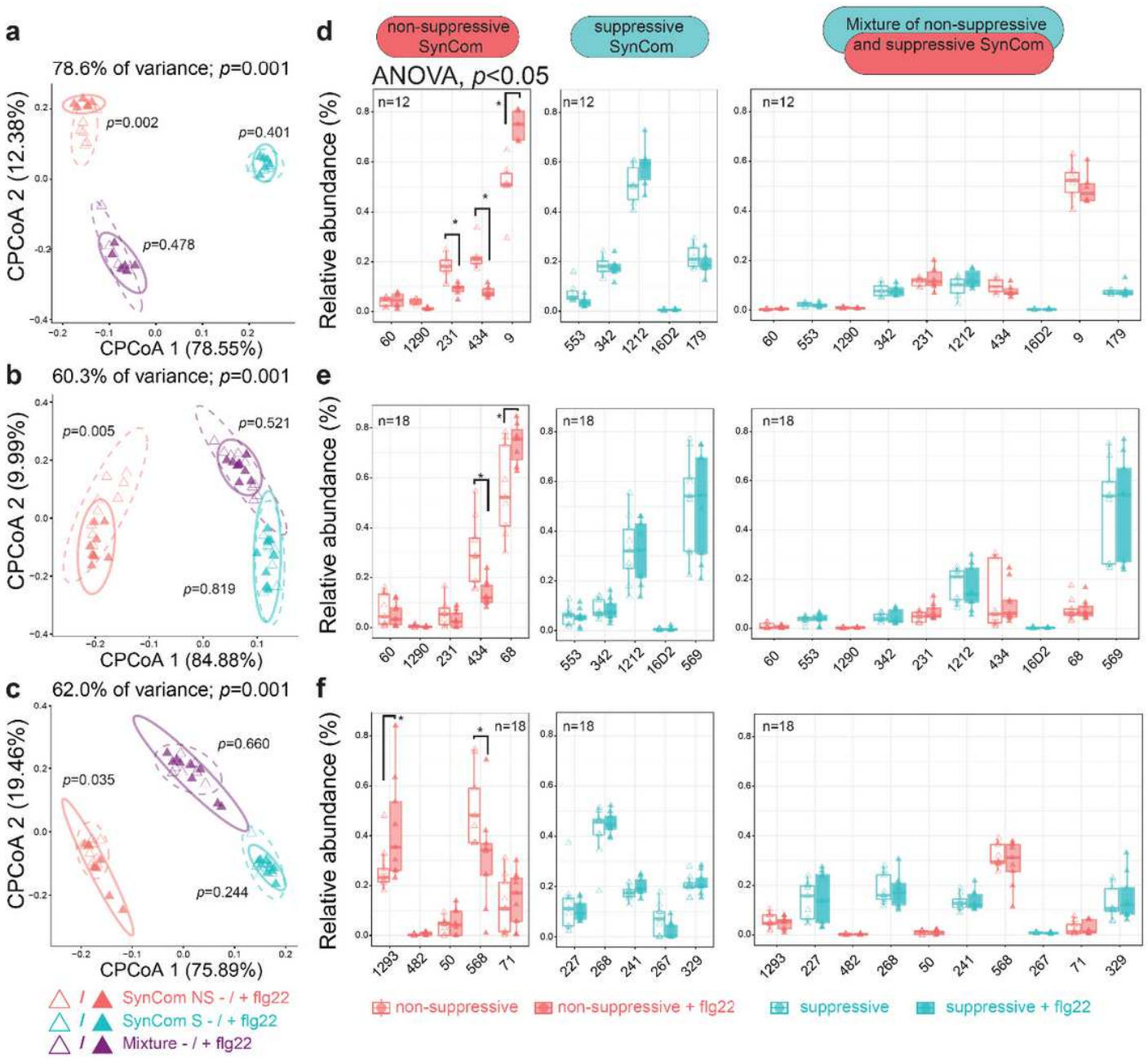


## Figure 2

Activation of immunity by flg22 affects community establishment. (a-c) Constrained coordination of the microbial profile of pWER::FLS2-GFP root samples showing the corresponding community shift of non-suppressive SynCom upon flg22 treatment. Ellipses correspond to Gaussian distributions fitted to each cluster (95% confidence interval). p-values next to ellipses indicate statistical significance based on a PERMANOVA test between untreated and flg22-treated samples of each SynCom (permutation=999). (d-f) Relative abundance of strains upon flg22 treatment. Experiment 1: (a,d); experiment 2: (b,e); experiment 3: (c,f). Values in bracket are eigenvalues explained by the Principal Component (PC). Asterisks indicate statistical significance.

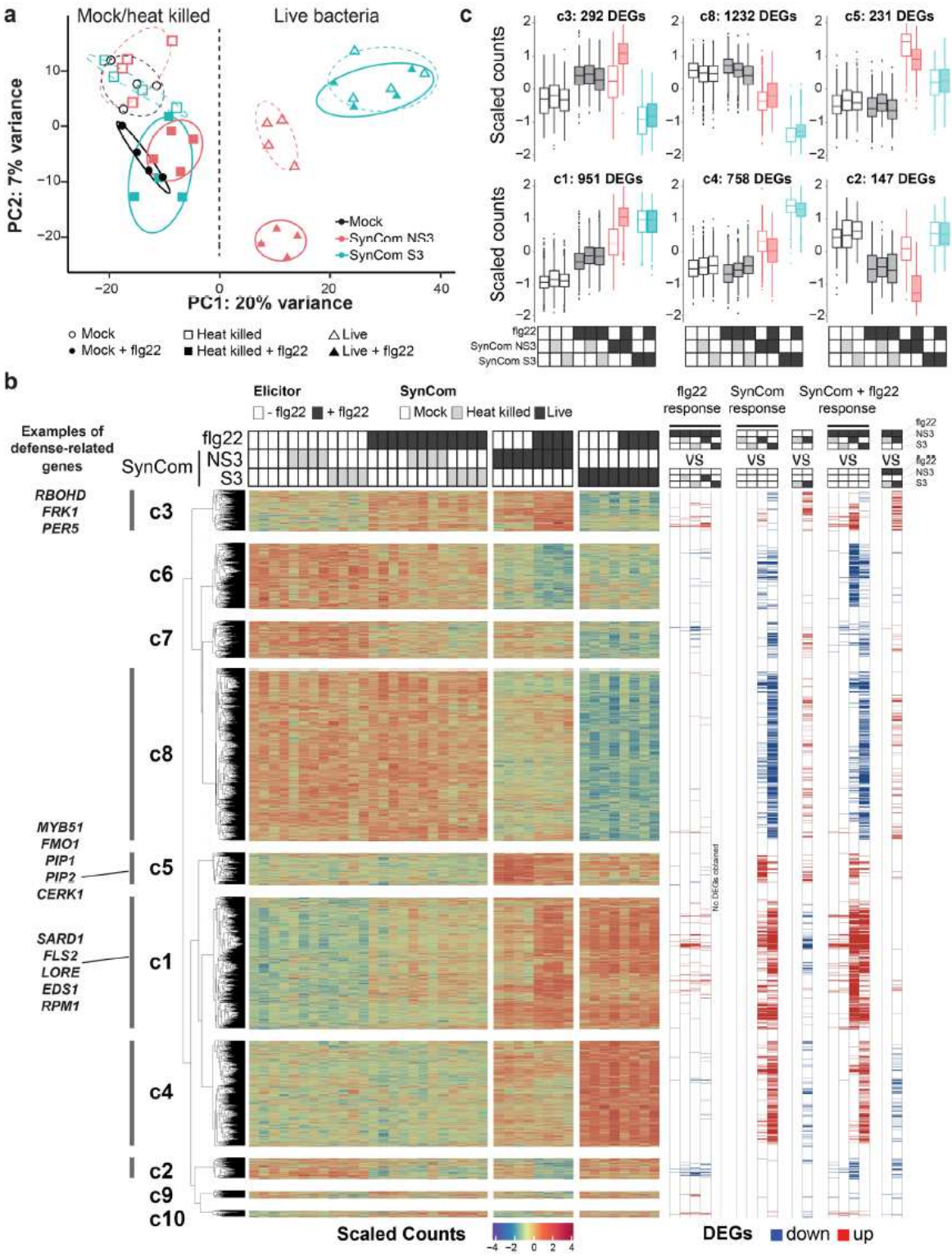


## Figure 3

SynCom colonization and flg22 treatment induce root transcriptomic changes in WT Col-0 plants. (a) PCA plot separating samples inoculated with SynComs and flg22. Ellipses correspond to t-distributions fitted to each cluster (70% confidence interval). (b) Heat map (middle) and DEGs (Table S3) obtained by pairwise comparison (right). k-means clusters (k = 10) are marked on the left. (c) Scaled counts of

transcripts in six clusters and their expression patterns upon treatments. The corresponding transcriptome data of pWER::FLS2-GFP plants are presented in Fig. S6 and table S2.

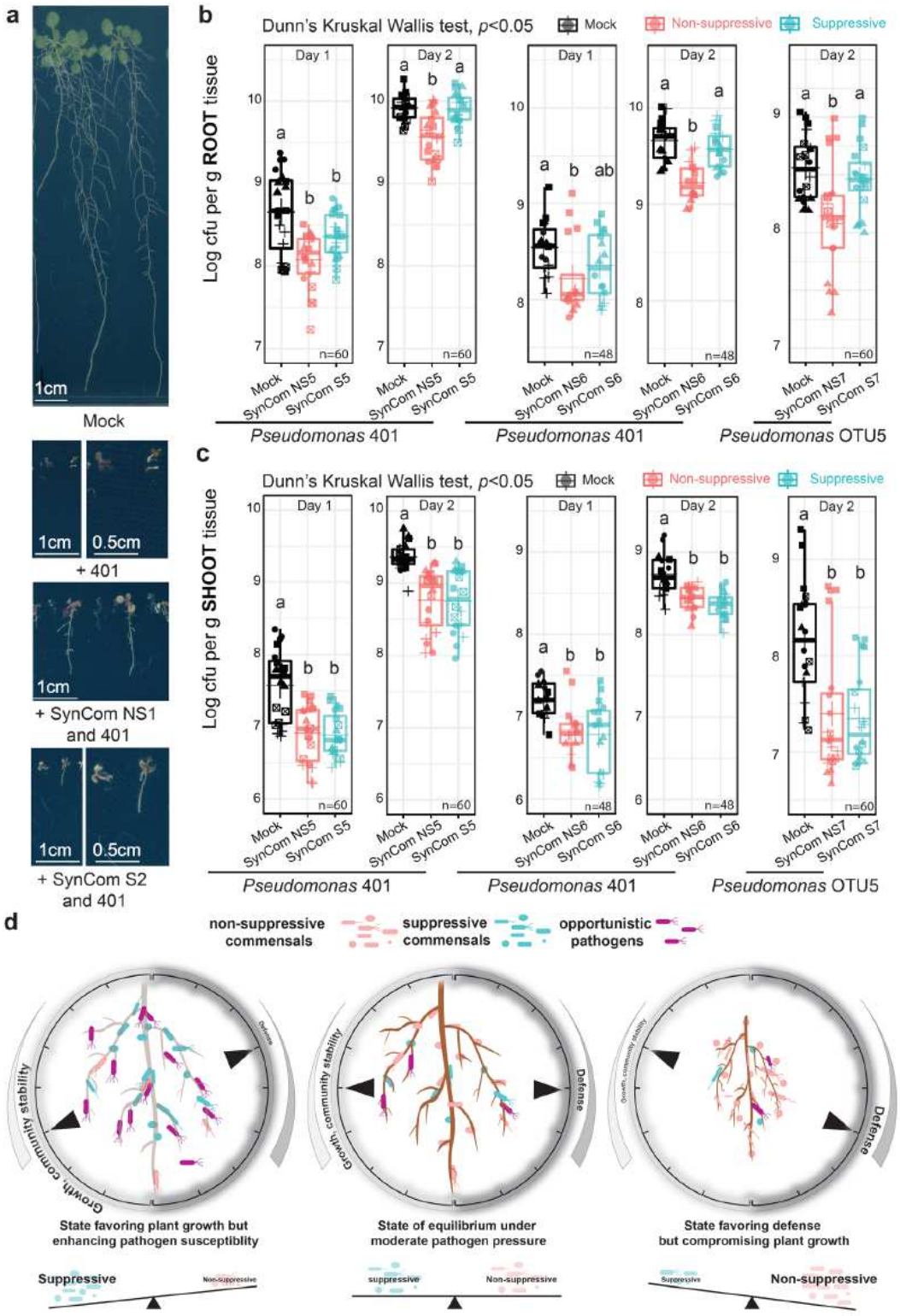


## Figure 4

Imbalance of specific bacteria impacts plant susceptibility to opportunistic Pseudomonas pathogens. (a) Symptoms of 3-week-old WT plants germinated with the indicated SynCom and Pseudomonas 401. Bacterial titer of Pseudomonas 401 and OTU5 on the roots (b) and shoots (c) of pWER::FLS2-GFP plants

pre-colonized with the indicated SynComs for 2 weeks. Shapes correspond to biological replicates. Different letters indicate statistical significance. (d) The “rheostat model” proposes that the balance between non-suppressive and suppressive strains integrates with plant innate immunity and buffers the system against pathogen challenge and defense-associated trade-off.

## Supplementary Files

This is a list of supplementary files associated with this preprint. Click to download.

- SIguide.pdf
- TableS1ListofSynComs.xlsx
- TableS2pWERRNASeq.xlsx
- TableS3Col0RNASeq.xlsx
- TableS4crossvalidation.xlsx
- TableS5Listofprimers.xlsx
- KaWaiMaetalfigurescombined.pdf